



HORIZON 2020

HORIZON 2020 RESEARCH AND INNOVATION FRAMEWORK PROGRAMME OF THE EUROPEAN ATOMIC ENERGY COMMUNITY

Nuclear Fission and Radiation Protection 2018 (NFRP-2018-4)

Project acronym: **SANDA**

Project full title: **Solving Challenges in Nuclear Data for the Safety of European Nuclear facilities**

Grant Agreement no.: **H2020 Grant Agreement number: 847552**

Workpackage N°: **WP2**

Identification N°: **D2.4**

Type of document: **Deliverable**


Title: **Report on the ^{239}Pu , ^{233}U , ^{14}N and $^{35,37}\text{Cl}$ inelastic cross section measurements at GELINA**

Dissemination Level: **PU**

Reference:

Status: **VERSION 1**

Comments:

	Name	Partner	Date	Signature
Prepared by:	A. Coman	10	24-07-2024	
WP leader:	D. Cano-Ott	1	04-07-2024	
IP Co-ordinator:	E. González	1	04-07-2024	

Report on the ^{239}Pu , ^{233}U , ^{14}N and $^{35,37}\text{Cl}$ inelastic cross section measurements at GELINA

Table of Contents

1.	Introduction.....	3
2.	Report on the measurements of $^{233}\text{U}(\text{n},\text{n}'\text{g})$ and $^{239}\text{Pu}(\text{n},\text{n}'\text{g})$ cross sections at GELINA using GRAPhEME.....	3
2.1	The prompt γ -ray spectroscopy method for (n, n') studies	4
2.2	Experimental conditions.....	4
2.3	$^{233}\text{U}(\text{n}, \text{n}'\gamma)$ cross section measurements.....	5
2.3.1	Upgrade of GRAPhEME.....	5
2.3.2	^{233}U sample.....	6
2.3.3	New data analysis procedure	6
2.3.4	(n, n' γ) cross sections	7
2.4	$^{239}\text{Pu}(\text{n}, \text{n}'\gamma)$ cross section measurements	10
3.	Report on the measurements of $^{14}\text{N}(\text{n},\text{n}'\text{g})$ and $^{35,37}\text{Cl}(\text{n},\text{n}'\gamma)$ cross sections at GELINA using GAINS	11
3.1	^{14}N (n,inl) cross sections.....	11
3.2	$^{35,37}\text{Cl}$ (n,inl) cross sections.....	14
4.	Report on the measurements of $^{182,184,186}\text{W}(\text{n},\text{n}'\text{g})$ cross sections at GELINA using GRAPhEME.....	15
4.1	Tungsten samples, measurement and data analysis.....	16
4.2	(n, n'g) cross sections	16
5.	Dissemination	18

1. Introduction

Within the scope of Task 2.3 (Neutron Elastic and Inelastic Scattering and Neutron Multiplication Cross Sections) under the SANDA project, it was proposed to perform neutron inelastic cross-section measurements on several isotopes critical for the development of nuclear facilities: ^{239}Pu , ^{233}U , ^{14}N , and $^{35,37}\text{Cl}$. These measurements were conducted at the GELINA (Geel Electron LINear Accelerator) neutron facility, operated by the EC-JRC in Geel, Belgium. The initiative responds to specific requirements for the development and design of the Generation IV nuclear reactors. Currently, there is a concerted effort to enhance existing nuclear technologies. The ultimate objective is to develop new types of nuclear facilities, such as Generation IV fast reactors and Accelerator-Driven Systems, which are expected to significantly address the prevalent issues in nuclear energy production. These issues include nuclear waste management, safety concerns, proliferation risks, and the abundance of nuclear fuel. A critical component of this initiative involves the nuclear data community providing highly accurate, reliable, and comprehensive neutron-induced cross-section datasets for a wide range of nuclei present within a nuclear reactor or produced during its normal operation. A particular focus is on the neutron inelastic channel, as it is the primary mechanism for neutron energy loss within the reactor. This channel also offers crucial information regarding gamma-ray sources and neutron flux attenuation, both of which are connected to radiation shielding and reactor criticality studies.

This report is structured into four sections, each detailing the current status of the corresponding measurement.

2. Report on the measurements of $^{233}\text{U}(\text{n},\text{n}'\gamma)$ and $^{239}\text{Pu}(\text{n},\text{n}'\gamma)$ cross sections at GELINA using GRAPhEME

Philippe Dessagne¹, Greg Henning¹, Maëlle Kerveno¹, Antoine Bacquias¹, Eliot Party¹, Gérard Rudolf¹, Pol Scholtes¹, Catalin Borcea², Marian Boromiza², Alexandru Negret², Adina Coman², Markus Nyman³, Carlos PARadela³, Arjan Plompen³, Roberto Capote⁴, Marc Dupuis⁵, Stephane Hilaire⁵, Pascal Romain⁵, Toshihiko Kawano⁶

¹Université de Strasbourg, CNRS, IPHC/DRS UMR 7178, Strasbourg, France

²Horia Hulubei National Institute of Physics and Nuclear Engineering, Magurele, Romania

³European Commission, Joint Research Centre, Geel, Belgium

⁴IAEA, Nuclear Data Section, Vienna, Austria

⁵CEA, DAM, DIF, F-91297 Arpajon, France

⁶Theoretical Division, Los Alamos National Laboratory, Los Alamos, NM 87545, USA

2.1 The prompt γ -ray spectroscopy method for (n, n') studies

Among the different experimental methods used for (n, xn) reaction studies, our collaboration has chosen the prompt γ -ray spectroscopy which, coupled with time-of-flight measurement allows the experimental determination of $(n, n'\gamma)$ cross section at the JRC-Geel GELINA facility. From the measured cross sections, the total neutron inelastic scattering and level production cross sections can be inferred as illustrated in Figure 1.

No se encuentra el origen de la referencia. 1. Innovative breeding fuel cycles, namely $^{232}\text{Th}/^{233}\text{U}$ and $^{238}\text{U}/^{239}\text{Pu}$ fuel cycles for Generation IV nuclear reactors selected by the Generation IV International Forum are very interesting because they extend available resources for thousands of years in the case of nuclear energy production. In this context, nuclear data of nuclei involved in such cycles must be known accurately to allow precise simulations of innovative reactor cores. Among all nuclear reactions that occur in the core, the (n, xn) reactions are of great importance because they modify the number of neutrons and their energy and if $x > 1$, they introduce new species inside the reactor core. Despite this need, there is today a lack of precise nuclear data, especially for those nuclei of interest. In particular, there is no experimental (n, xn) reaction cross section data for the fissile nucleus ^{233}U and for the case of ^{239}Pu , only a very few data exist at limited neutron energies.

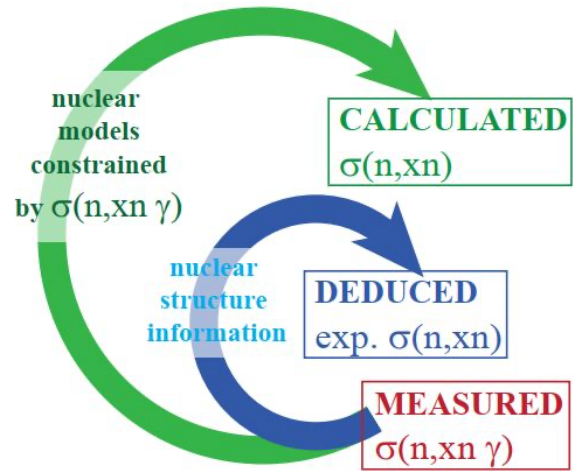


Figure 1: Schematic view of the two ways to deduce total (n, xn) cross section from measured $(n, n'\gamma)$ ones. From reference [1].

2.2 Experimental conditions

The GRAPhEME setup is installed at 30 m from the EC JRC-Geel GELINA neutron source, a distance that appeared to be a good compromise between neutron energy resolution and available actinides quantities for sample making. During previous measurement campaigns (^{232}Th , ^{235}U , ^{238}U , W, Zr), it was composed of four planar HPGe detectors surrounded by a Pu-Cd-Cu shielding to protect the Germanium crystal from neutron and γ backgrounds. The HPGe crystals have a typical thickness around 2-3 cm and a diameter around 5-6 cm. They are placed around the sample at 110° and 150° with regards to the neutron beam to allow the precise angular integration of the γ -ray production cross sections. A fission chamber, loaded with a thin layer of ^{235}U ($^{235}\text{UF}_4$ with an areal density of $0.324(2) \text{ mg/cm}^2$), is present upstream GRAPhEME and is used for neutron flux determination. The signals (time and energy) from the detectors are recorded by a digital acquisition system based on TNT2 cards [2] (14 bits for amplitude resolution and a 100 MHz sampling frequency) except for the ^{239}Pu measurement (cf. section 4). The efficiency of each HPGe detector has been precisely studied with source measurements (^{152}Eu) coupled with MCNPX [3] simulations. To take into account the spatial distribution of the neutron beam (55 mm in diameter), source measurements have been performed with point sources at different positions relative to the centre of the beam and also with an extended source. If the sample is radioactive, the radioactive decay can also be used for efficiency calibration. Once the detectors' geometry is well-defined, the production for each γ transition is simulated including the sample of interest to take into account the self-absorption of the γ 's in the sample. For the fission chamber, as described in reference [4], its operation has

been optimized to maximize the efficiency of detection. For additional details, the readers can also refer to the D.2.5 report.

2.3 $^{233}\text{U}(n, n'\gamma)$ cross section measurements

2.3.1 Upgrade of GRAPhEME

To deal with the high radioactivity of the sample and the high fission cross section, GRAPhEME has been upgraded with a segmented (36 pixels) HPGe detector. With its high γ -energy resolution and the reduction of pile-up events due to the segmentation, it allows a good γ identification and separation of γ events from (n, n') , (n, f) reactions and radioactivity of the sample become possible. This capability is illustrated in Figure 3.

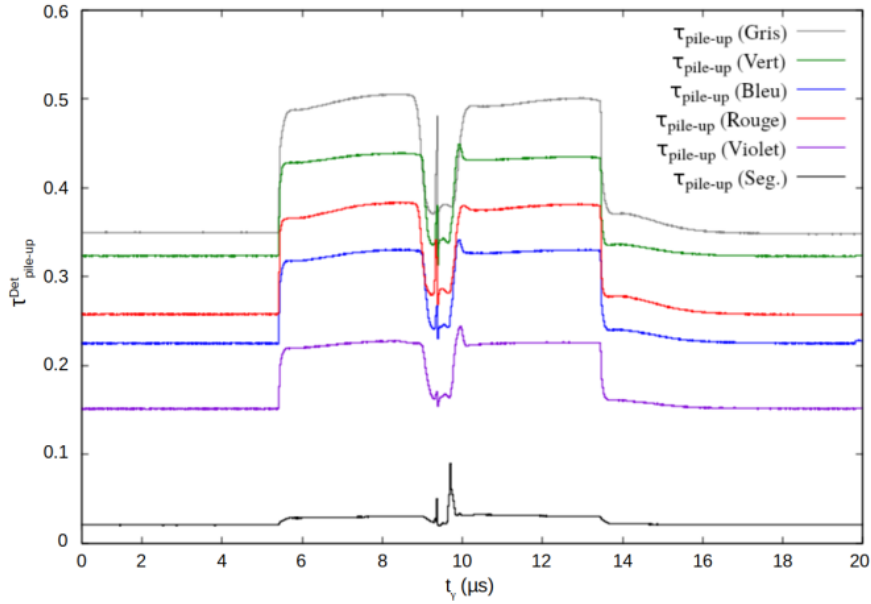


Figure 2: pile-up rate as a function of the detector and as a function of time. Figure from [5].

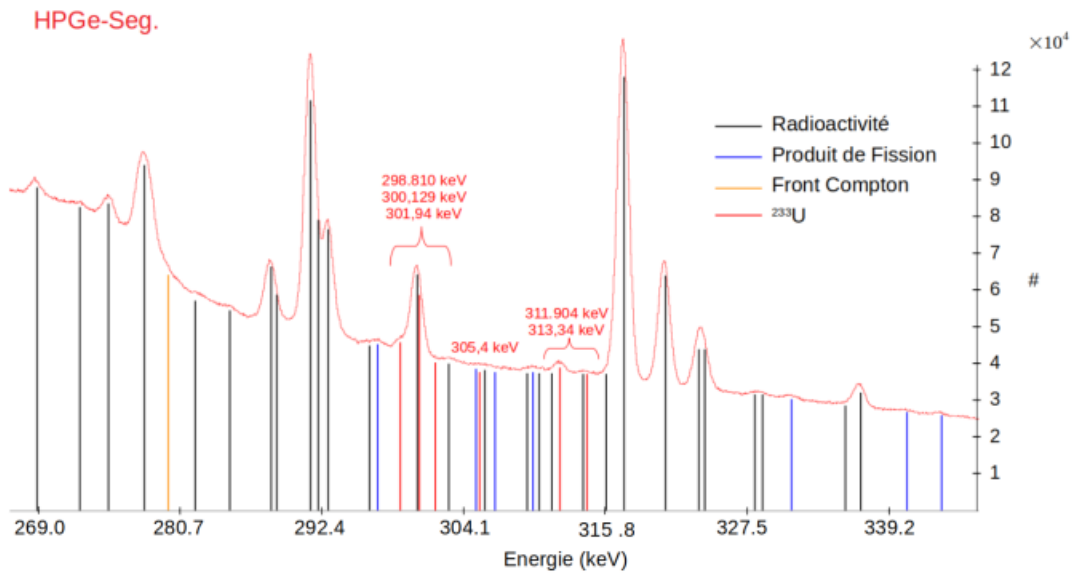


Figure 3: Portion of the energy spectrum for $E_\gamma \in [270, 375]$ keV in the neutron inelastic scattering energy region obtained with the Segmented HPGe detector. Are identified and marked 28 radioactivity γ rays (in black), 7 γ transitions from a fission

product (in blue), a Compton edge from a very intense γ ray at 440 keV (in orange) and 6 γ rays of interest coming from (n, n' γ) reaction on ^{233}U . (in red) Figure from [5].

2.3.2 ^{233}U sample

The sample has been provided by the SCK-CEN (Studie Centrum voor Kernenergie) Mol, in Belgium. It is a metallic disk, with a diameter of 30 mm and a thickness of 640 μm . In total, it has a mass of 8.1936 g (measured by the EC-JRC-Geel). This pellet is stored in a hermetic container that allows safe handling of the sample. Figure 4 shows a picture of the ^{233}U sample in its container seen from the front side.

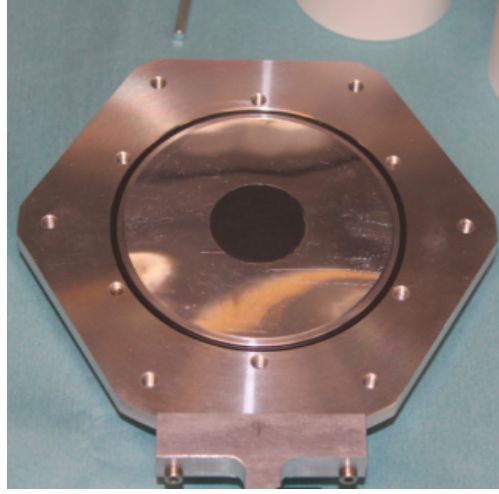


Figure 4 : Photo of the sample inside its support.

The sample is made out of Uranium-dioxide UO_2 . It is thus crucial to determine the number of target ^{233}U nuclei only for the purpose of the data analysis. To do so, off-beam radioactivity measurements are performed to measure the number of ^{233}U nuclei present in the sample. ^{233}U decays to ^{229}Th emitting α particles. Thanks to the structure data of radioactive decay given in ENSDF, namely γ energies and intensities, the total number of disintegrated nuclei can be known. Finally, knowing the half-life of the nucleus of interest, the total number of ^{233}U nuclei in the target can be deduced:

$$m_{^{233}\text{U}} = 7.85 (5) \text{ g}, \quad N_{^{233}\text{U}} = 2.87 (1) 10^{21} \text{ nuclei.cm}^{-2}$$

2.3.3 New data analysis procedure

To improve our data analysis procedure and obtain a better treatment of uncertainty propagation, we have developed a new software based on a semi-Monte-Carlo (sMC) tool and called Resimulator [6]. We chose the Python computing language to implement this tool, using the libraries *NUMPY* and *MATPLOTLIB*, for calculations and representation of results respectively. In this case, correlations and covariance matrices are easy to obtain since *NUMPY* contains packages that compute them, namely *NUMPY.CORRCOEFF* and *NUMPY.COV*. The working principle of this tool is the following: From the data analysis, we have extracted all parameters involved in the cross section formula with their associated uncertainties. Then, we perform N random draw of each parameter, following a Gaussian distribution of mean value, standard deviation and area equal to N . A differential cross section is calculated at each iteration for each angle and each detector. The two differential cross sections are then combined using the Gauss quadrature [1]. We thus obtain a Gaussian distribution of the cross section. Parameters of this distribution are extracted. Its central value is the value of the (n, n' γ) cross section and its standard deviation is its uncertainty. The validation of the method has been made on ^{238}U data

sets and published in [6]. An example of correlation matrix obtained for a γ -transition cross section is given in Figure 5.

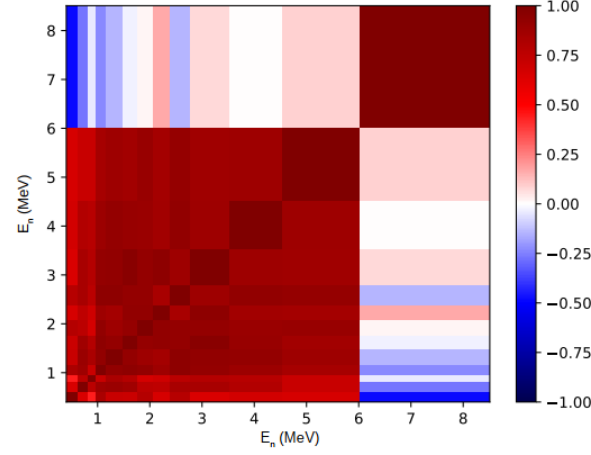


Figure 5 : correlation matrix obtained for γ -transition cross section in ^{233}U , $E_\gamma=311.9 \text{ keV}$.

2.3.4 (n, n' γ) cross sections

The data collection for ^{233}U sample represents a total acquisition time of 4794 hours. During such long periods, instabilities might occur. Moreover, GELINA is only operational five days a week (shut down during weekends) and there are two shut down periods during summer and winter. Thus, the very first step of the data analysis is checking data, adjusting them and building raw data sets. Indeed, with such long acquisition time and such numerous acquisition cards involved, instabilities can arise and has to be corrected (shift in time for TOF spectra and gain adjustment for energy spectra). From the whole amount of obtained data, we manage to build 3 data sets for different detectors which corresponds to 4519, 3865.3 and 3823 hours.

With these statistics, we were able to extract 12 γ transitions in ^{233}U corresponding to the (n, n') process. The list of the γ rays is given in

Table 1.

Table 1 : γ transitions from $^{233}\text{U}(n, n'\gamma)$ reactions observed and for which the cross section data have been calculated. Structure information from the nuclear database ENSDF is given for each transition.

E_γ (keV) Mesurée	E_γ (keV) Données de [87]	État initial		État final		I_γ	M_γ
		J^π (h)	E_i (keV)	J^π (h)	E_f (keV)		
260.6 (9)	261.4 (2)	$(\frac{5}{2}^-)$	301.94 (9)	$\frac{7}{2}^+$	40.351 (7)	100	/
280.5 (9)	280.58 (5)	$\frac{7}{2}^-$	320.77 (5)	$\frac{7}{2}^+$	40.351 (7)	100 ± 12	/
288.2 (9)	288.33 (10)	$(\frac{7}{2}^+)$	380.38 (8)	$\frac{9}{2}^+$	92.15 (4)	100 ± 10	/
298.9 (9)	298.81 (2)	$(\frac{5}{2}^-)$	298.815 (10)	$\frac{5}{2}^+$	0.0	100.0 ± 2.5	/
300.2 (9)	300.128 (10)	$\frac{5}{2}^+$	340.378 (6)	$\frac{7}{2}^+$	40.351 (7)	100.0 ± 1.0	M1+E2
301.8 (9)	301.99 (10)	$(\frac{5}{2}^-)$	301.94 (9)	$\frac{5}{2}^+$	0.0	67	/
305.4 (9)	305.4 (2)	$\frac{3}{2}^+$	397.55 (21)	$\frac{9}{2}^+$	92.15 (4)	100	/
312.0 (9)	311.901 (10)	$\frac{3}{2}^+$	311.906 (6)	$\frac{5}{2}^+$	0.0	100.0 ± 1.0	M1+E2
313.9 (9)	313.34 (20)	$\frac{9}{2}^-$	353.78 (12)	$\frac{7}{2}^+$	40.351 (7)	100 ± 6	/
340.8 (9)	340.477 (10)	$\frac{5}{2}^+$	340.378 (6)	$\frac{5}{2}^+$	0.0	67.9 ± 0.7	M1+E2
376.9 (9)	375.407 (10)	$\frac{3}{2}^+$	415.761 (7)	$\frac{7}{2}^+$	40.351 (7)	39.1 ± 0.4	E2
415.4 (9)	415.764 (10)	$\frac{3}{2}^+$	415.761 (7)	$\frac{5}{2}^+$	0.0	100.0 ± 1.1	M1+E2

The $(n, n'\gamma)$ cross sections obtained for the 12 γ rays are presented in *Figure 6* and *Figure 7*. They are compared to nuclear reaction code calculations only, as no experimental data exists. As it can be seen, room for improvement of calculations exists.

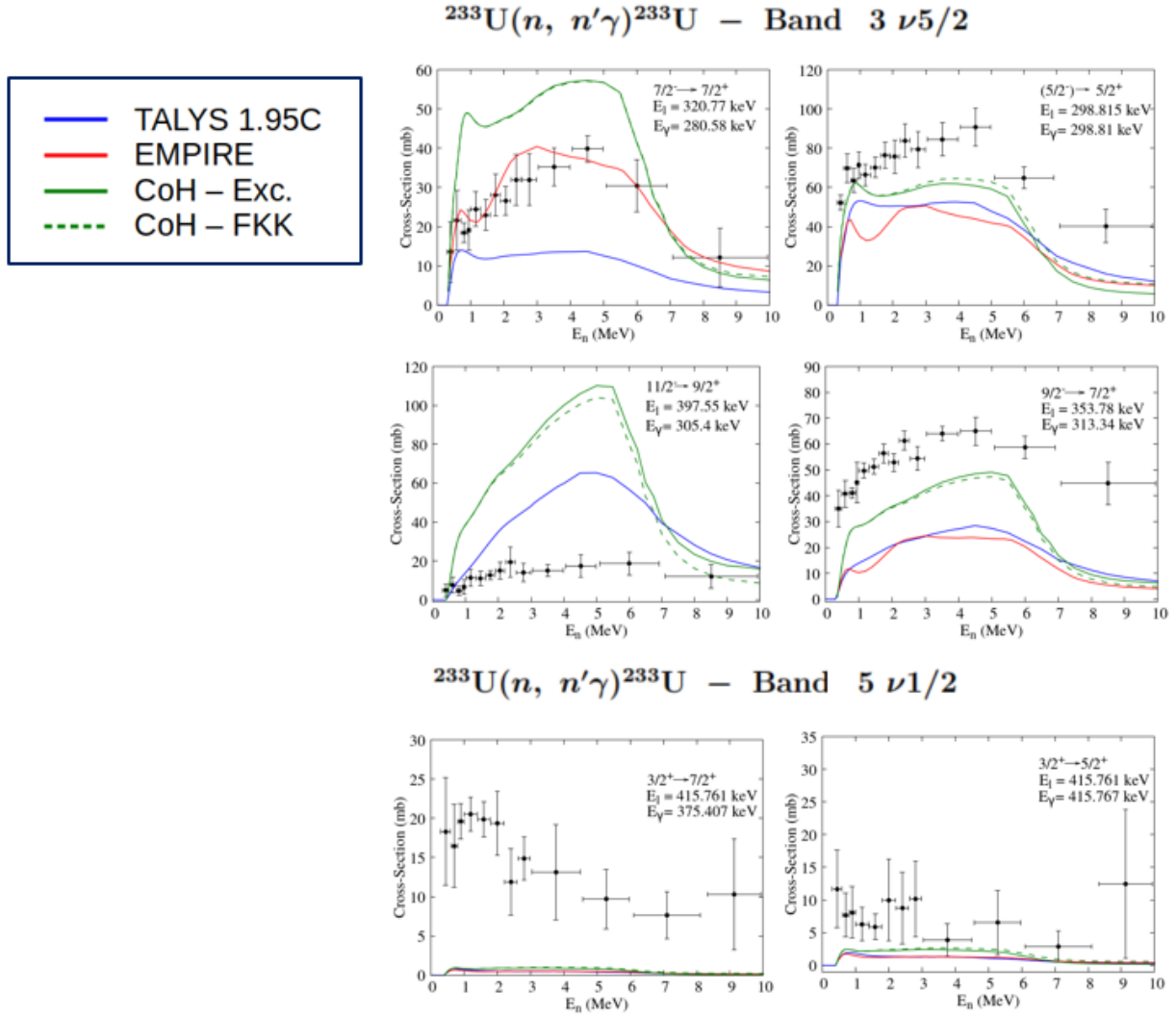


Figure 6 : Experimental $^{233}\text{U}(n, n'\gamma)$ cross sections for transition from band 3 and 5 levels as a function of the incident neutron energy E_n and compared to nuclear reaction codes calculations TALYS (with best parameters see [5]), EMPIRE and two calculations of CoH with classical and microscopic treatment of preequilibrium process.

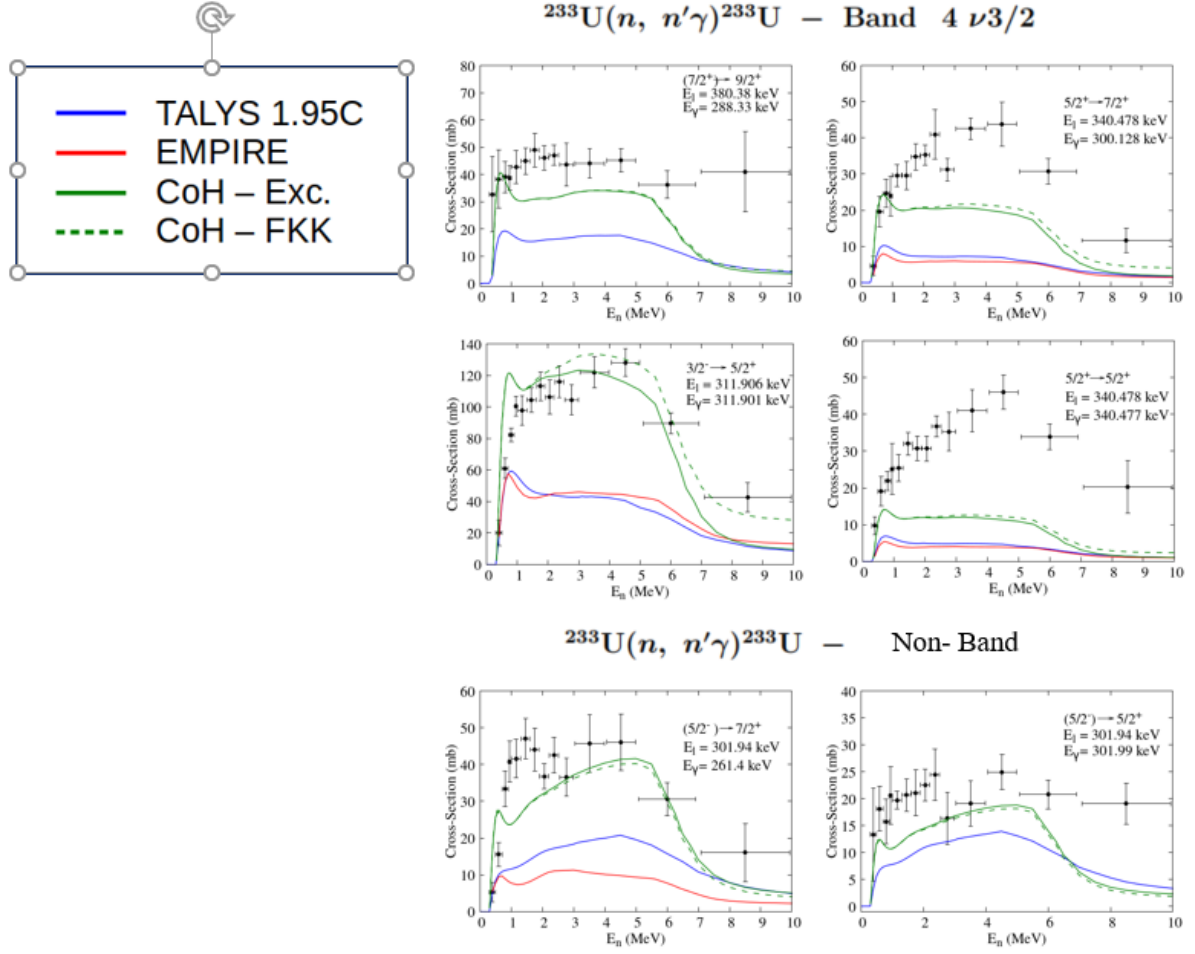


Figure 7 : Experimental $^{233}\text{U}(n, n'\gamma)$ cross sections for transition from band 4 and non band levels as a function of the incident neutron energy E_n and compared to nuclear reaction codes calculations TALYS (with best parameters see [5]), EMPIRE and two calculations of CoH with classical and microscopic treatment of preequilibrium process.

2.3.1 Branching ratios

An important ingredient in the prompt γ ray spectroscopy method is the good knowledge of the nuclei structure information. With our measurements, when we are able to measure the deexcitation of a level by several γ rays, we can deduce the γ intensity and check the value in the ENSDF database [7]. We have calculated γ intensity for all levels where it was possible, and the results are summarized in Table 2 where discrepancies are observed.

Table 2 : Experimental γ intensities obtained in this work compared to ENSDF.

Initial state		Final states			I_γ	
$E_{i,l}$ (keV)	J_i^π (\hbar)	E_γ (keV)	$E_{f,l}$ (keV)	J_f^π (\hbar)	I_γ (Exp.)	I_γ (ENSDF)
301.94	$(\frac{5}{2}^-)$	261.4	40.351	$\frac{7}{2}^+$	100	100
		301.99	0.0	$\frac{5}{2}^+$	50.48 ± 3.34	67
340.478	$\frac{5}{2}^+$	300.128	40.351	$\frac{7}{2}^+$	100	100
		340.477	0.0	$\frac{5}{2}^+$	95.42 ± 4.92	67.9 ± 8.5

2.4 $^{239}\text{Pu}(n, n'\gamma)$ cross section measurements

The challenge of this measurement was the making of the sample. Indeed, this project requires a sample as free as possible from ^{241}Am which is built from the decay of ^{241}Pu present in the sample. From the PuO_2 powder provided by EC-JRC Geel, SCK-CEN (Mol Belgium) managed to reduce by a factor of 10^{-4} the activity ratio $^{241}\text{Am}/^{239}\text{Pu}$, which reaches finally the value of $\sim 1.5 \times 10^{-4}$. With this material, EC JRC-Geel has prepared a sample with a mass of 2.3 g, a diameter of ~ 5 cm and a thickness around 0.1 cm [8]. This task, under the supervision of WP3 of the SANDA project, suffered from delays caused by the COVID pandemic. We received the sample during the spring 2022.

Then the GRAPhEME data acquisition system (DAQ) was upgraded from TNT to FASTER (<https://faster.in2p3.fr>), see Figure 8.

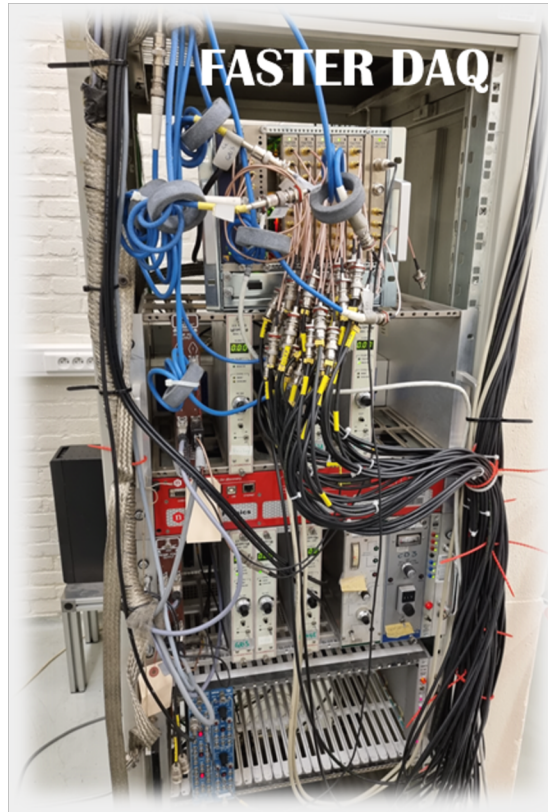


Figure 8 : photo of the FASTER data acquisition system coupled with the GRAPhEME spectrometer.

Following the Ukraine war and the increase of electricity cost in 2022-2023, the JRC-Geel facility has reduced the operation time in 2023 and unfortunately, the accelerator suffered a severe breakdown when restarted in September 2023. No beam was then available up to now. Before the stop of GELINA operation, we had a few weeks of beam that we have used for the new DAQ settings, the real start of acquisition period was planned for September 2023 but did not take place. We are thus not in the possibility to produce any cross section data for this deliverable even preliminary results. It has to be recall that this kind of measurement requires several thousand hours of beam time in very good conditions (see section 3) and we are very far from this situation today.

As soon as the GELINA neutron beam will restart, we will perform the measurement but it will be outside the time frame of the SANDA project.

3. Report on the measurements of $^{14}\text{N}(n,n'\gamma)$ and $^{35,37}\text{Cl}(n,n'\gamma)$ cross sections at GELINA using GAINS

Catalin Borcea¹, D. Chiriac¹, Marian Boromiza¹, Alexandru Negret¹, Adina Coman¹, Philippe Dessagne², Greg Henning², Maëlle Kerveno², Markus Nyman³, A. Oprea³, Carlos Paradelo³, Arjan Plompen³

¹Horia Hulubei National Institute of Physics and Nuclear Engineering, Magurele, Romania

²Université de Strasbourg, CNRS, IPHC/DRS UMR 7178, Strasbourg, France

³European Commission, Joint Research Centre, Geel, Belgium

3.1 ^{14}N (n,inl) cross sections

Nitride fuels (like UN, UN₂...) have been proposed for liquid-metal-fast-breeder reactors (LMFBRs) because of their good reactor performance in terms of high melting point, high thermal conductivity, fabricability, high fissile density (e.g., 40% more uranium per molecule in UN compared to UO₂, which is typically used), and easier reprocessing via the PUREX method. Nitrogen-based minor actinides compounds (such as NpN, AmN, etc.) are also being studied as viable candidates for use in Accelerator-Driven Systems (ADS) as part of the minor actinides recycling process. The presence of non-actinides (such as nitrogen, oxygen, carbon, etc.) in the fuel impacts fuel density and increases parasitic absorption and moderation of neutrons, which negatively affects neutron economy. Even though ^{14}N constitutes 99.63% of natural nitrogen (with ^{15}N only making up 0.36%), the latter is actually preferred for nitride-based nuclear fuel because neutron capture on ^{14}N produces the highly toxic ^{14}C . Enriching nitride fuel with the ^{15}N isotope reduces both its radiotoxicity and parasitic absorption within the reactor core. ^{14}N is also produced via the (n,d) reaction on ^{15}N , but the cross-section of this reaction is approximately 13 times smaller than that of the (n,p) reaction on. Despite enrichment efforts, small quantities of ^{14}N remain in the fuel. Therefore, it is important to also characterize the neutron inelastic channel on ^{14}N by measuring, for instance, the gamma-production cross-sections for the most intense transition arising from this isotope.

The inelastic channel measurement on nitrogen-14 is part of an EUFRAT open access project. This experiment was performed at the GELINA neutron source, using the GAINS spectrometer (see Figure 9) located in the 100-meter measurement cabin on flight path 3. Data collection began in the latter half of 2022, albeit with a delay primarily caused by the COVID-19 pandemic and the subsequent (and necessary) maintenance to restart the accelerator.

For this measurement, GELINA operated at 400 Hz, employing all 12 HPGe detectors of the spectrometer. The detectors were placed at 110°, 150° and 125° with respect to the beam direction, with four detectors positioned at each angle, at distances ranging from 16 to 18 cm from the target. These angles enable accurate integration of the gamma ray's angular distribution as $\cos(110^\circ)$ and $\cos(150^\circ)$ correspond to the nodes of the fourth-degree Legendre polynomials [9]. The detectors exhibit a typical gamma energy resolution of 2.3 keV for the 1332-keV peak of ^{60}Co , and 100% relative efficiency.

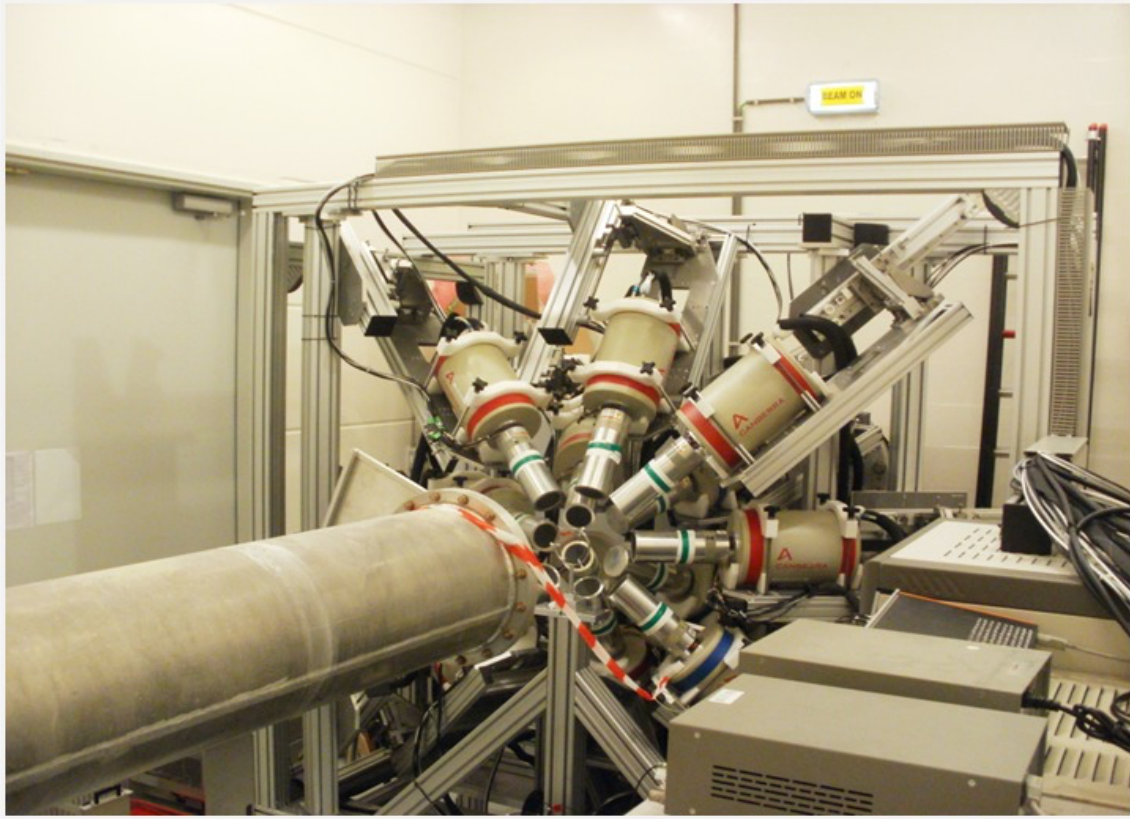


Figure 9: The Gamma Array for Inelastic Neutron Scattering (GAINS) Spectrometer at the 100-m measurement station of the GELINA neutron source in Geel.

The incident neutron flux was monitored using a ^{235}U -filled fission chamber located 211.15 cm upstream the sample. Within the measurement cabin, the energy-integrated neutron flux yielded approximately 770 neutrons per square centimeter per second and the neutron beam was collimated to a diameter of 61.00(50) mm.

The HPGe detectors were read out using DC440 Acqiris digitizers, which operate at a sampling rate of 420 million samples per second, with a 12-bit amplitude resolution. The waveforms are transferred to PCs, where the signal processing is performed online by in-house developed data acquisition software. For each signal, we record both the time and amplitude. The time correlates with the energy of the neutron that induced the reaction, while the amplitude is proportional to the gamma energy. A neutron energy resolution of approximately 3 keV at 1 MeV and up to around 80 keV at 10 MeV is achieved.

The sample being irradiated was a silicon nitride (Si_3N_4), with a thickness of 4 mm and dimensions of 100 mm by 100 mm. The presence of silicon in the sample allows for a cross-validation of the results, as we have previously measured this isotope.

The data analysis procedure is detailed extensively in Refs. [10-12] and will not be repeated here.

Following data analysis, we constructed amplitude spectra where we were able to observe with reasonable statistics only two γ transitions (at 2312.5 and 1635.2 keV) coming from the neutron inelastic scattering on ^{14}N . For each transition we calculated the γ -production cross section. A difficulty of this experiment was gathering the desired statistics due to a two-fold reason: the aftermath of the COVID pandemic, which affected both the accelerator and the research team,

coupled with the small inelastic channel associated to this (very) light target nucleus (the main transition barely reaches 200 mb, see below). This translated to large uncertainties of the reported data, especially above 10 MeV where the GELINA neutron flux drops considerably. The reported data have uncertainties around 10-20%.

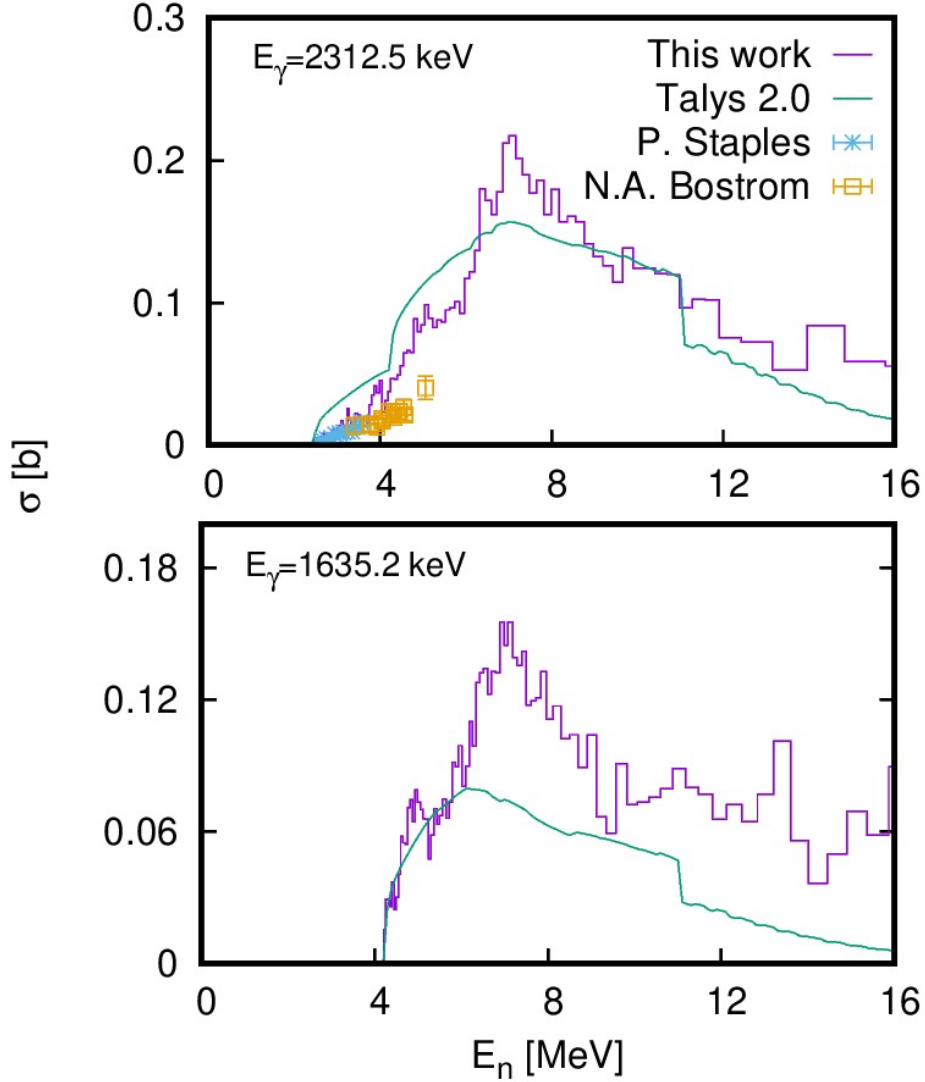


Figure 10: The production cross sections of the first two transitions in ^{14}N compared with previously available experimental points taken from the EXFOR data base and the TALYS 2.0 [13] default input theoretical calculations.

Our results for the two main transitions in ^{14}N are displayed in Figure 10 and compared with previously reported data taken from EXFOR and with TALYS 2.0 default settings theoretical predictions [13]. Staples et al. [14] and Bostrom et al. [15] measured only the first transition using quasi-monoenergetic neutron beams generated by the $^7\text{Li}(p,n)$ reaction and the reported values have large uncertainties (as high as 50%). Moreover, the authors employed only one detection angle (i.e., 125 degrees) for the angular integration of the differential data. The data set provided by our group is the first time-of-flight inelastic data for this isotope, with very good neutron energy resolution, which extends across the entire range of incident energies relevant for the inelastic channel (E_{th} up to 16 MeV), see Figure 10. We also provide for the first-time inelastic data for the second transition, at 1635.2 keV. Despite a very good agreement with the Staples et al. [14] and Bostrom et al. [15] cross section values for the main transition near the

threshold region, soon after we report larger cross section values (considerably outside the error bars of the 3 measurements). The theoretical prediction in this region seems to follow the trend of our data even though soon after the codes start to underpredict the experimental results (see especially the case of the 1635.2 keV gamma ray above 6 MeV incident energy). Nonetheless, the fact that a statistical model-based reaction code employed with default settings/parameters is able to describe such a light nuclear mass system is actually impressive.

3.2 $^{35,37}\text{Cl}$ (n,inel) cross sections

Fast neutron spectrum Molten Salt Reactors (MSRs) are highly promising for future energy production due to their compact and safer nuclear energy capabilities. These reactors utilize molten salt as both nuclear fuel carrier and coolant and are well-suited for operating with thorium-bearing fuel, which acts as fertile material, and offer a potential solution for recycling and transmuting the large stockpiles of plutonium and minor actinides accumulated in the spent fuel up to now. Historically, fluoride salts have been the primary choice for MSR designs, but, recently, there has been growing interest in chloride salts as a compelling alternative for such nuclear facilities. One motivation arises from the fact that chloride salts enable reactor operation at lower temperatures compared to fluoride-based mixtures. Also, sodium chloride (NaCl), commonly known as rock salt, is an abundant resource available in geological deposits and the ocean, presenting an attractive alternative to lithium, which is a scarce resource in high demand. Overall, the use of chlorine salts in molten salt nuclear reactors holds great promise for improving the safety, efficiency, and sustainability of nuclear power technologies. Therefore, the precise knowledge of the neutron-induced cross sections on the stable isotopes of chlorine is crucial for the design and development of MSRs. Because inelastic scattering is the main neutron energy-loss mechanism in a reactor, it is very important to know very accurate the γ -ray production cross sections following this reaction in a large incident energy range.

Chlorine has two stable isotopes: ^{35}Cl and ^{37}Cl with abundances of 75.76(10)% and 24.24(10)%, respectively [16]. The High Priority Request List (HPRL) [17] of NEA has currently an entry dedicated to several reaction channels of ^{35}Cl , including the (n,p) channel for incident energies up to more than 19 MeV.

In conclusion, a better knowledge of the neutron inelastic cross sections on the stable isotopes of Chlorine will aid the community in lowering the sensitivity of the overall k_{eff} uncertainty for this type of nuclear facilities.

The main objective of the experiment is to produce γ -production cross sections associated to the inelastic scattering reaction on both stable isotopes of Chlorine. These are the primary results of our experiment. Another objective is to use these quantities, together with information about the known level scheme of the target nuclei, to also calculate level and total inelastic cross sections. We expect to extract cross sections with total uncertainties below 5-8% for the strongest transitions.

The experiment will be performed using the same facility, experimental setup and data analysis procedure to the ones already detailed in Section 4 above. One important difference is the DAQ as we plan to measure in parallel with two digital systems: the older DC440 Acqiris used thus far and a new Struck SIS3316 digitizer [20]. This will allow us to cross-check the performance of the new Struck digitizers (which we plan to use moving forward).

The target, already available at JRC Geel, consists of an 80x3 mm NaCl disk canned in a 0.2 mm thickness Aluminium container. The corresponding areal density is 0.247 g/cm² for ^{35}Cl and 0.079 g/cm² for ^{37}Cl , respectively.

A simple calculation, performed using the TALYS 2.0 code [13] with default input parameters, predicts reasonable intensity for the inelastic channel and at least 3 γ -ray transitions from each isotope (see Figs. Figure 11Figure 14) following inelastic scattering. The energies of the

transitions are well suited for HPGe detectors. We also used TALYS to estimate the most intense competing channels on $^{35,37}\text{Cl}$ for 100 keV to 20 MeV incident energies (see Figure 11Figure 12). We note that the residual nuclei of these reactions do not emit gamma rays with overlapping energies with the ones of interest. One can see that, together with the inelastic, the (n,p) and (n,a) channel have fairly large cross sections.

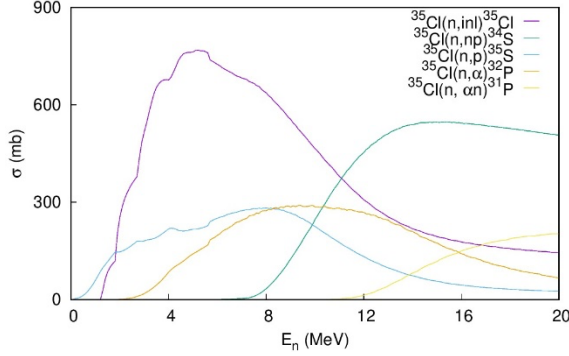


Figure 11: The most intense neutron induced reaction channels on ^{35}Cl as calculated using the TALYS 2.0 code with default input parameters.

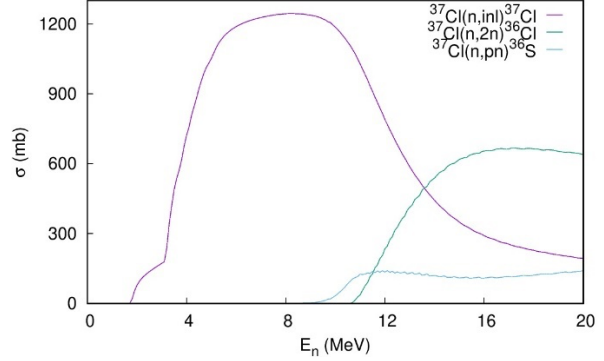


Figure 12: The most intense neutron induced reaction channels on ^{37}Cl as calculated using the TALYS 2.0 code with default input parameters.

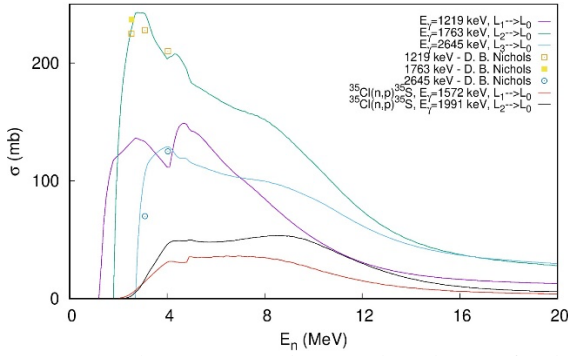


Figure 13: The TALYS 2.0 theoretical predictions for the most intense γ -ray transitions in ^{35}Cl (with lines) and the EXFOR available experimental results (with points).

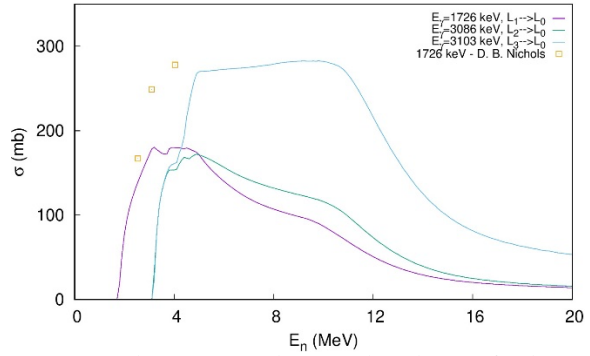


Figure 14: The TALYS 2.0 theoretical predictions for the most intense γ -ray transitions in ^{37}Cl (with lines) and the EXFOR available experimental results (with points).

Figure 13Figure 14 display previously measured experimental values found in the Experimental Nuclear reaction data base (EXFOR) for the inelastic channel of $^{35,37}\text{Cl}$. As one can see, the data is very scarce and not in a good agreement with the TALYS 2.0 default theoretical predictions. The experiment will be the first one to determine neutron inelastic cross section values with very good neutron energy resolution (3 keV at 1 MeV and 80 keV at 10 MeV) and for a range that covers the entire incident energy domain relevant for the inelastic channel on this target nucleus (0.5-20 MeV). This accurate and reliable data will, in turn, impact all future evaluations performed for chlorine and increase the overall quality of these nuclear data with direct consequences for Molten Salt Reactor design and ultimately in the development of cleaner energy production.

4. Report on the measurements of $^{182,184,186}\text{W}(n,n'\gamma)$ cross sections at GELINA using GRAPhEME

During the time frame of the SANDA project, we have analyzed datasets coming from a previous measurement campaign done on even isotopes of tungsten. As a mitigation of the problem encountered with the ^{239}Pu and $^{35,37}\text{Cl}$ measurements, we propose to provide

$^{182,184,186}\text{W}(n, n'\gamma)$ cross sections. The three proposed isotopes are replaced with the three even stable isotopes of tungsten.

4.1 Tungsten samples, measurement and data analysis

The High-purity tungsten samples of isotopes $^{182,184,186}\text{W}$ were placed separately in the GRAPhEME setup, with an independent measurement campaign for each. An additional measurement with a natural tungsten sample was made and allow a cross-check and normalization of the results.

The γ -ray spectra were recorded, focusing on the energy resolution of the γ -rays. The detectors were calibrated using known radioactive sources. This data was then used to determine the cross-sections of various γ -ray production reactions. The conditions of these experiments were the same as for the ^{238}U measurement. Please refer to the D2.5 report for a detailed description. The recorded spectra were analyzed to identify γ -ray peaks corresponding to known transitions in the nuclei of interest. The cross-sections were calculated by relating the observed γ -ray yields to the neutron flux. Corrections were applied for factors such as detector efficiency, background radiation, and neutron flux variations.

The data was analyzed using a Random Sampling method to account for all uncertainty parameters [6]. This allows the production of final uncertainties that reflect the measurement constraints in the most accurate way [21].

4.2 (n, n' γ) cross sections

The (n, n' γ) cross sections for 70 transitions in the $^{182,184,186}\text{W}$ were determined this way (24, 19 and 27 for the respective isotopes), with 19 of them being confirmed with measurements in the natural tungsten sample.

As no other data set of this type is currently known, it was not possible to compare our results to previous measurements, but comparison to reaction code predictions was possible (Talys [13], Empire [22], and CoH3 [23]).

Some results are shown, as illustration in Figures 15-18.

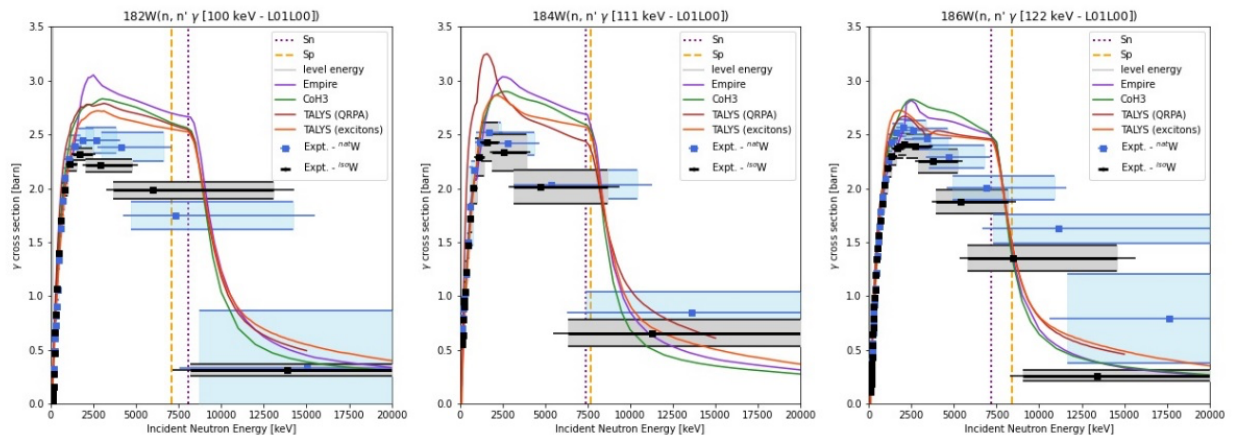


Figure 15 : Experimental (n, n' transition) cross sections for the first excited state (2^+) to ground state (0^+) in the 182, 184 and 186 tungsten isotopes, extracted from the isotopically enriched target data set (black) and natural tungsten target (blue). The experimental values are compared to prediction from Talys (red and orange), Empire (purple) and CoH3 (green). For information, the S_p and S_n values are visualized with vertical dashed lines (yellow, purple) and the threshold energy is marked with a gray vertical line (hidden by the Y-axis here).

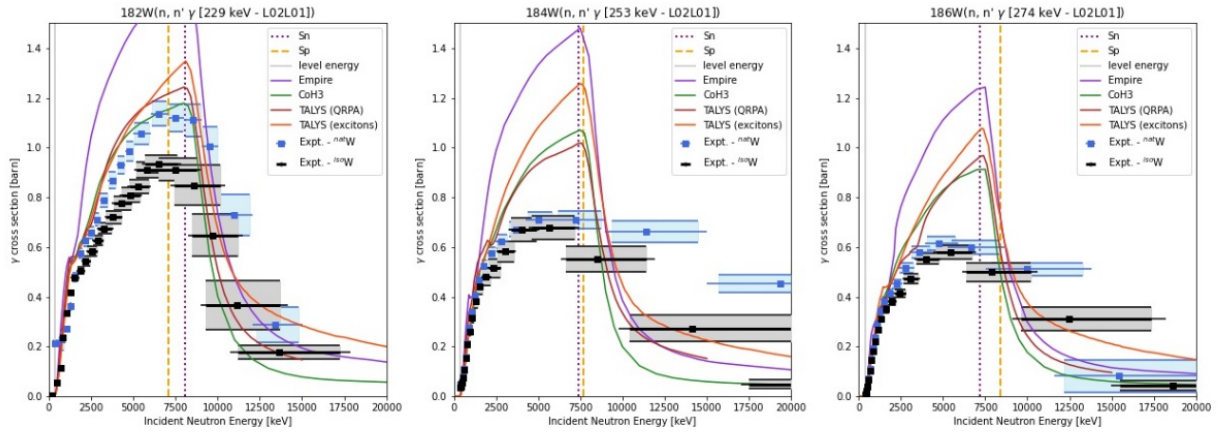


Figure 16 : Same as Fig. 9, for the transition from the 4^+ state in the fundamental rotational band, to the first excited state (2^+).

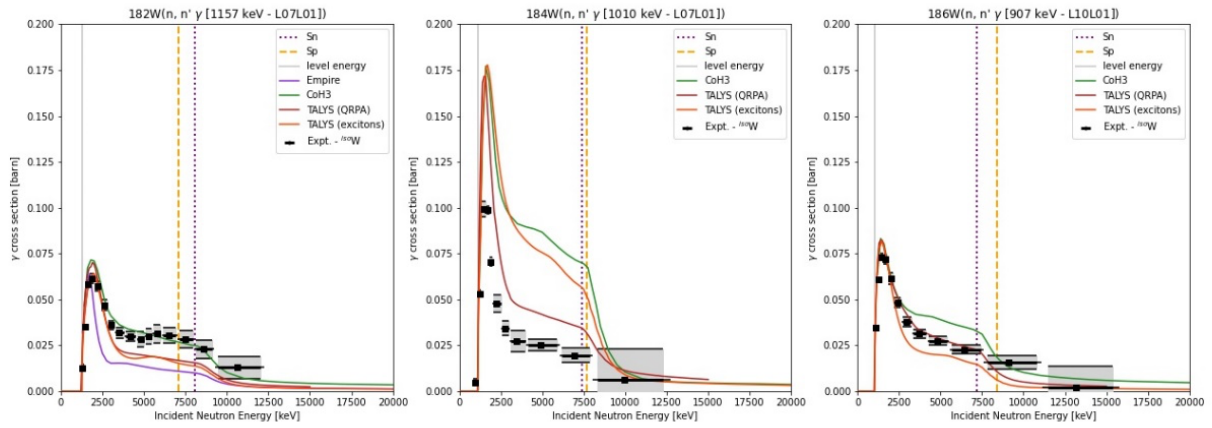


Figure 17 : Same as Fig. 9, for the transition from the 2^+ state in the β band, to the first excited state (2^+).

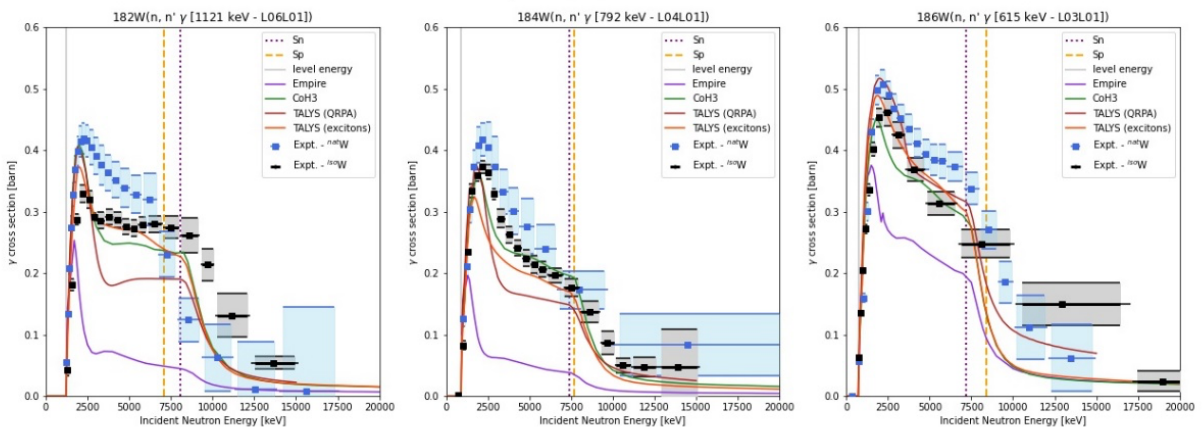


Figure 18 : Same as Fig. 10, for the transition from the 2^+ state in the γ band, to the first excited state (2^+).

The compatibility of the theoretical values with the experimental ones is mixed, depending on the transitions. However, it is not in any significant way better or worse than the results seen in previous studies [4,5,24,25]. We have a strong collaboration with theoreticians, in the frame of

which we are looking into what model parameters can be fine-tuned to increase the predicting power of the codes.

This extensive data set, including several isotopes of increasing mass, is a very valuable testing ground for the reaction models and will help improve them significantly.

5. Dissemination

Publications

- *GRAPhEME: performances, achievements (@EC-JRC/GELINA) and future (@GANIL/SPIRAL2/NFS)*

M. Kerveno, et al., EPJ Web of Conferences 284, 01005 (2023)

hal-04221754v1

<https://doi.org/10.1051/epjconf/202328401005>

- *The past and the future of the GAINS spectrometer @ GELINA*

A. Olacel et al., EPJ Web of Conferences 284, 01007 (2023)

<https://doi.org/10.1051/epjconf/202328401007>

- *Neutron-induced inelastic γ -production cross sections on $^{58,60,64}\text{Ni}$*

M. Boromiza et al., EPJ Web of Conferences 284, 01010 (2023)

<https://doi.org/10.1051/epjconf/202328401010>

- *Measurement of partial $(n,n'\gamma)$ reaction cross sections on highly radioactive nuclei of interest for energy production application*

F. Claeys et al., EPJ Web of Conferences 284, 01014 (2023)

<https://doi.org/10.1051/epjconf/202328401014>

- *Nucleon-induced inelastic cross sections on ^{nat}Ni*

A. Olacel, et al., Phys. Rev. C 106, 024609 (2022)

<https://doi.org/10.1103/PhysRevC.106.024609>

- *Measurement of $^{238}\text{U}(n, n'\gamma)$ cross section data and their impact on reaction models*

M. Kerveno, M. Dupuis, et al. Physical Review C 104, 044605 (2021)

hal-03382914v1

<https://dx.doi.org/10.1103/PhysRevC.104.044605>

- *Measurement of $^{182,184,186}\text{W}(n, n'\gamma)$ cross sections and what we can learn from it*

G. Henning, et al., EPJ Web of Conferences, 247, 09003 (2021)

hal-03197274v1

<https://dx.doi.org/10.1051/epjconf/202124709003>

- *What can we learn from $(n,xn\gamma)$ cross sections about reaction mechanism and nuclear structure ?*

M. Kerveno, M. Dupuis, et al. Eur. Phys. J Web of Conferences 239, 01023 (2020)

hal-02957494

<https://dx.doi.org/10.1051/epjconf/202023901023>

- *Measurement of $(n, xn\gamma)$ reaction cross sections in W isotopes*

Greg Henning, et al. EPJ Web Conf., 146, 11016 (2017)

hal-02154835v1

<https://doi.org/10.1051/epjconf/201714611016>

- *Measurement of (n, xng) reaction cross sections in W isotopes.*

G Henning et al. - 14th International Conference on Nuclear Reaction Mechanisms, Villa Monastero, Varena, Italy, 15 - 19 Jun 2015, pp.247

Conferences/workshops -

- ND2019: International Conference on Nuclear Data for Science and Technology 2019, 19-24 May 2019, Beijing, China

- ND2022: International Conference on Nuclear Data for Science and Technology 2022, 24-29 July 2022, Sacramento, USA, remotely with Gathertown

- WINS2023: Workshop on Elastic and Inelastic Neutron Scattering (WINS-2023), October 10th, 2023 to October 12th, 2023, Troy, US.

- 14th International Conference on Nuclear Reaction Mechanisms, Villa Monastero, Varenna, Italy, 15 - 19 Jun 2015.

Nuclear data/cross sections

- The cross sections data for ^{233}U measurements are available in reference [5]. This work has been the thesis subject of F. Claeys at the University of Strasbourg. The article relative to this work is in preparation and will be submitted to Physical Review C. As soon as the paper will be published the cross section data will be sent to the EXFOR database.

- The differential γ -production cross sections for the first transition in ^{14}N , which are the primary experimental results, are listed in Annex 1. The angle-integrated γ -production cross sections will be submitted to EXFOR once the article it is published.

- The experimental data obtained from the inelastic neutron scattering measurements on tungsten isotopes $^{182,184,186}\text{W}$ is publicly available under the [Etalab Open License](https://etalab.gouv.fr/licence-ouverte-open-licence/) (<https://etalab.gouv.fr/licence-ouverte-open-licence/>), (compatible [CC-BY](https://creativecommons.org/licenses/by/4.0/deed.en) <https://creativecommons.org/licenses/by/4.0/deed.en>). This open data publication includes detailed cross-sections for 63 γ -ray production channels. The data is published on the [Recherche Data Gouv](https://recherche.data.gouv.fr/fr) French platform (<https://recherche.data.gouv.fr/fr>) [26], and currently under embargo, pending the publication of a scientific article currently in preparation. The data will also be sent to the [EXFOR](https://www-nds.iaea.org/exfor/) portal (<https://www-nds.iaea.org/exfor/>).

References

1. M. Kerveno et al. Eur. Phys. J. N 4, 23, (2018).
2. L. Arnold, R. Baumann, E. Chambit, M. Filliger, C. Fuchs, C. Kieber, D. Klein, P. Medina, C. Parisel, M. Richer et al., in 14th IEEE-NPSS Real Time Conference, 2005 (IEEE, Piscataway, NJ, 2005), pp. 265–269.
3. MCNPX, online: <http://mcnpx.lanl.gov/>
4. M. Kerveno, et al, Phys. Rev. C 87, 024609 (2013).

5. F. Claeys, “Mesure, modélisation et évaluation de sections efficaces à seuil (n, xn) d'intérêt pour les applications de l'énergie nucléaire”. Thèse de doctorat, 2023. <https://theses.fr/2023STRAE027>
6. G. Henning et al., EPJ Web of Conferences 284, 01045 (2023)
7. E. Browne and J. Tuli, Nucl. Data Sheets 127, 191 (2015).
8. A. Moens et al. EPJ Web of Conf. 285, 04002 (2023)
9. C. R. Brune, Nucl. Instrum. Methods Phys. Res. A 493, 106 (2002).
10. A. Coman et al., Phys. Rev. C 90, 034603 (2014).
11. A. Coman, PhD Thesis, University of Bucharest, faculty of Physics (2015).
12. M. Boromiza, A. Coman et al., Phys. Rev. C 90, 034603 (2014).
13. A. Koning, S. Hilaire and S. Goriely, Eur. Phys. J. A 59, 131 (2023).
14. P. Staples, J.J.Egan, G.H.R.Kegel, A.Mittler, Nuclear Science and Engineering, Vol.126, p.168 (1997).
15. N. A. Bostrom, I.L.Morgan, J.T.Prud'homme, P.L.Okhuysen, A.R.Sattar, Wright Air Devel. Centre Reports, No.58-88 (1958).
16. J. Meija, T. B. Coplen, M. Berglung, W. A. Brand, P. De Bièvre, M. Groning, N. E. Holden, J. Irrgeher, R. D. Loss, T. Walczyk, and T. Prohaska, Pure Appl. Chem. 88, 293 (2016).
17. <https://www.oecd-neo.org/dbdata/hppl/search.pl?vhp=on>
18. <https://world-nuclear.org/information-library/current-and-future-generation/molten-salt-reactors>
19. K. Lawson, and N. R. Brown, Nuclear Technology, 1–18 (2024).
20. A. Coman et al., Proceedings for the “15th International Conference on Nuclear Data for Science and Technology (ND2022)”, EPJ Web of Conferences 284, 01007 (2023).
21. G. Henning, et al. EPJ Web Conf. 247, 09003 (2021)
22. M. Herman, R. Capote, B.V. Carlson, P. Oblozinsky, M. Sin, A. Trkov, H. Wienke, V. Zerkin, “EMPIRE: Nuclear Reaction Model Code System for Data Evaluation”, Nucl. Data Sheets, 108 (2007) 2655-2
23. T. Kawano (2021). CoH3: The Coupled-Channels and Hauser-Feshbach Code. In: Escher, J., et al. Compound-Nuclear Reactions. Springer Proceedings in Physics, vol 254. Springer, Cham.
24. M. Kerveno, M. Dupuis, et al. Physical Review C 104, 044605 (2021)
25. E. Party et al., EPJ Web of Conferences 211, 03005 (2019)
26. G. Henning, (2024), "Experimental (n, n' gamma) cross sections for isotopes ^{182}W , ^{184}W and ^{186}W ", <https://doi.org/10.57745/JRCNEJ>, Recherche Data Gouv

ANNEX 1

1. The differential γ production cross section for the 2312-keV transition in ^{14}N at 110°

Time of flight (ns)	E_n (keV)	$ds/d\Omega$ (b/sr)	uncertainty $ds/d\Omega$ (b/sr)
4637.25	2424.36	0.000249577	0.000147749
4608.67	2454.63	0.000224795	0.000265862
4580.1	2485.48	0.000225069	0.000129828
4551.53	2516.9	0.000374524	0.000136438
4522.96	2548.93	0.000262705	0.000134757
4494.39	2581.58	0.000216599	0.000156823
4465.82	2614.86	0.000561389	0.000157037
4437.25	2648.78	0.000354352	0.000155086
4408.67	2683.37	0.0004955	0.000223051
4380.1	2718.65	0.000629442	0.000179428
4351.53	2754.62	0.000614132	0.000187158
4322.96	2791.32	0.000662944	0.000188024
4294.39	2828.75	0.000507541	0.000199959
4265.82	2866.94	0.000523191	0.000191503
4237.25	2905.92	0.000564115	0.000213016
4208.67	2945.69	0.000696345	0.000198825
4180.1	2986.29	0.000712097	0.000209969
4151.53	3027.74	0.000969702	0.000237982
4122.96	3070.05	0.00106731	0.000245166
4094.39	3113.26	0.0013496	0.000258882
4065.82	3157.39	0.00110733	0.000264481
4037.25	3202.47	0.00117422	0.000266814
4008.67	3248.52	0.00208012	0.000309278
3980.1	3295.57	0.00154387	0.000286814
3951.53	3343.66	0.00117053	0.000328751
3922.96	3392.81	0.00136635	0.000363428
3894.39	3443.05	0.00169491	0.000361181
3865.82	3494.41	0.00159259	0.000342501
3837.25	3546.94	0.00129838	0.000353794
3808.67	3600.66	0.00115887	0.000353353
3780.1	3655.62	0.00105553	0.000348387
3751.53	3711.85	0.00131124	0.000411602
3722.96	3769.38	0.00198202	0.000404971
3694.39	3828.27	0.00284062	0.000457625
3665.82	3888.55	0.00370686	0.000455145
3637.25	3950.27	0.00296692	0.000406454
3608.67	4013.47	0.00305501	0.000534177
3580.1	4078.2	0.00189466	0.00042202
3551.53	4144.52	0.00228448	0.000469145

3522.96	4212.47	0.00259402	0.000439682
3494.39	4282.11	0.00337744	0.000476479
3465.82	4353.5	0.00388644	0.000462271
3437.25	4426.69	0.00448165	0.000491694
3408.67	4501.75	0.00430432	0.000493366
3380.1	4578.73	0.00533726	0.000529515
3351.53	4657.71	0.00530376	0.000551289
3322.96	4738.76	0.00516345	0.00054897
3294.39	4821.95	0.00671415	0.000601693
3265.82	4907.36	0.00584687	0.000602804
3237.25	4995.06	0.00700543	0.000629036
3208.67	5085.14	0.00772838	0.000680248
3180.1	5177.68	0.00653302	0.000633928
3151.53	5272.78	0.00604723	0.000629666
3122.96	5370.54	0.0066588	0.000655984
3094.39	5471.04	0.00655155	0.000655264
3065.82	5574.41	0.00753212	0.000662339
3037.25	5680.73	0.0072552	0.000646661
3008.67	5790.14	0.00780725	0.000644147
2980.1	5902.75	0.00703688	0.000623566
2951.53	6018.69	0.00908951	0.000699233
2922.96	6138.09	0.010059	0.000721537
2894.39	6261.09	0.0102848	0.000738857
2865.82	6387.84	0.0147325	0.000889206
2837.25	6518.49	0.0133461	0.000866519
2808.67	6653.2	0.0120475	0.000825238
2780.1	6792.15	0.0138134	0.000904734
2751.53	6935.51	0.0159165	0.000996303
2722.96	7083.48	0.0162958	0.000999403
2694.39	7236.25	0.0157662	0.00100291
2665.82	7394.04	0.0145435	0.000980363
2637.25	7557.07	0.0137895	0.000979551
2608.67	7725.57	0.0145723	0.00102201
2580.1	7899.8	0.0117798	0.000979241
2551.53	8080.01	0.014382	0.00104301
2522.96	8266.49	0.0118847	0.00101644
2494.39	8459.52	0.012515	0.00102301
2465.82	8659.43	0.0119064	0.00103894
2437.25	8866.55	0.00995417	0.00100005
2408.67	9081.22	0.0104248	0.00104688
2380.1	9303.83	0.0102578	0.00112549
2351.53	9534.76	0.00984936	0.00111695
2322.96	9774.44	0.0108918	0.00124918
2294.39	10023.3	0.0100808	0.00123386

2265.82	10281.9	0.00986432	0.00128266
2237.25	10550.7	0.00961692	0.0013928
2208.67	10830.2	0.00853803	0.00141392
2180.1	11121	0.00805098	0.00137385
2151.53	11423.8	0.00718937	0.00165889
2122.96	11739.1	0.00835139	0.00158483
2094.39	12067.9	0.00624977	0.00110562
2037.25	12768.4	0.00524932	0.00116067
1980.1	13532.2	0.00379163	0.00144381
1922.96	14367.2	0.00627218	0.00146054
1865.82	15282.6	0.00477979	0.00198387
1808.67	16289.2	0.00277929	0.00166444
1751.53	17399.6	0.00358877	0.00152699

2. The differential γ production cross section for the 2312-keV transition in ^{14}N at 150°

Time of flight (ns)	E_n (keV)	$ds/d\Omega$ (b/sr)	uncertainty $ds/d\Omega$ (b/sr)
4637.25	2424.36	3.09475e-05	0.000154927
4608.67	2454.63	0.00039727	0.000170674
4580.1	2485.48	1.06703e-05	0.000176432
4551.53	2516.9	0.000539867	0.000153943
4522.96	2548.93	0.000320342	0.000169919
4494.39	2581.58	0.000242481	0.000232219
4465.82	2614.86	0.000197184	0.00019251
4437.25	2648.78	0.000709282	0.000229404
4408.67	2683.37	0.000943559	0.000298813
4380.1	2718.65	0.000659762	0.000227792
4351.53	2754.62	0.000488997	0.000270571
4322.96	2791.32	0.000592044	0.00021877
4294.39	2828.75	0.000617272	0.000270175
4265.82	2866.94	0.000678848	0.000212779
4237.25	2905.92	0.0014571	0.000306426
4208.67	2945.69	0.00054522	0.000310574
4180.1	2986.29	0.00115688	0.000251133
4151.53	3027.74	0.00100643	0.000279851
4122.96	3070.05	0.00115425	0.000279294
4094.39	3113.26	0.00139536	0.000346096
4065.82	3157.39	0.00107203	0.000306738
4037.25	3202.47	0.00067851	0.000361199
4008.67	3248.52	0.00196283	0.000339141
3980.1	3295.57	0.0011054	0.000379061
3951.53	3343.66	0.000880731	0.000362471
3922.96	3392.81	0.00121131	0.000398697
3894.39	3443.05	0.0018769	0.000464122

3865.82	3494.41	0.00191813	0.000484163
3837.25	3546.94	0.00116094	0.000497042
3808.67	3600.66	0.00197973	0.000470087
3780.1	3655.62	0.00224229	0.000515806
3751.53	3711.85	0.00127061	0.00056801
3722.96	3769.38	0.00283011	0.000563849
3694.39	3828.27	0.00272421	0.000511224
3665.82	3888.55	0.00255486	0.000539153
3637.25	3950.27	0.00292808	0.000537713
3608.67	4013.47	0.00465513	0.000678792
3580.1	4078.2	0.00183578	0.000518827
3551.53	4144.52	0.00295009	0.000585678
3522.96	4212.47	0.0037919	0.000610271
3494.39	4282.11	0.00432649	0.000644591
3465.82	4353.5	0.00333694	0.000591812
3437.25	4426.69	0.00292381	0.000613532
3408.67	4501.75	0.00472125	0.000640792
3380.1	4578.73	0.00485699	0.000667168
3351.53	4657.71	0.00529589	0.000679657
3322.96	4738.76	0.00524946	0.000658782
3294.39	4821.95	0.00776391	0.000719154
3265.82	4907.36	0.00727554	0.000717682
3237.25	4995.06	0.00617255	0.000733363
3208.67	5085.14	0.00806816	0.00079195
3180.1	5177.68	0.00820342	0.00081521
3151.53	5272.78	0.00763733	0.000830317
3122.96	5370.54	0.00762753	0.000828275
3094.39	5471.04	0.00749417	0.000822388
3065.82	5574.41	0.00760311	0.000850583
3037.25	5680.73	0.00851896	0.000820039
3008.67	5790.14	0.00841466	0.000789171
2980.1	5902.75	0.00804851	0.000807447
2951.53	6018.69	0.00974509	0.000851079
2922.96	6138.09	0.00898365	0.000805361
2894.39	6261.09	0.0120415	0.000877916
2865.82	6387.84	0.013555	0.000940143
2837.25	6518.49	0.0142898	0.000976521
2808.67	6653.2	0.0145125	0.000991752
2780.1	6792.15	0.0148542	0.00101562
2751.53	6935.51	0.0187359	0.00114943
2722.96	7083.48	0.0191531	0.00118436
2694.39	7236.25	0.0165113	0.00113555
2665.82	7394.04	0.016216	0.00113864
2637.25	7557.07	0.0146342	0.00112191

2608.67	7725.57	0.0152465	0.00115479
2580.1	7899.8	0.014968	0.001177
2551.53	8080.01	0.0141883	0.00117661
2522.96	8266.49	0.0135801	0.00117949
2494.39	8459.52	0.0133233	0.00113613
2465.82	8659.43	0.0136151	0.00121456
2437.25	8866.55	0.0136909	0.00125466
2408.67	9081.22	0.0107834	0.00123317
2380.1	9303.83	0.00963677	0.00135323
2351.53	9534.76	0.00774948	0.00128269
2322.96	9774.44	0.0112662	0.00140144
2294.39	10023.3	0.00953941	0.00143629
2265.82	10281.9	0.00994742	0.0015272
2237.25	10550.7	0.00959895	0.00153839
2208.67	10830.2	0.0114275	0.0016877
2180.1	11121	0.00698064	0.00157663
2151.53	11423.8	0.00999202	0.00188084
2122.96	11739.1	0.00773549	0.00176264
2094.39	12067.9	0.0055556	0.0012911
2037.25	12768.4	0.00674018	0.0014256
1980.1	13532.2	0.0049743	0.00180458
1922.96	14367.2	0.00753028	0.00214693
1865.82	15282.6	0.00452858	0.0022429
1808.67	16289.2	0.00751385	0.00187006
1751.53	17399.6	0.00202357	0.0019274

3. The differential γ production cross section for the 2312-keV transition in ^{14}N at 125°

Time of flight (ns)	E_n (keV)	$ds/d\Omega$ (b/sr)	uncertainty $ds/d\Omega$ (b/sr)
4637.25	2424.36	4.83662e-05	0.000133478
4608.67	2454.63	0.000265647	0.00020013
4580.1	2485.48	0.000112593	0.000142206
4551.53	2516.9	0.000117621	0.000163154
4522.96	2548.93	0.000246933	0.000138744
4494.39	2581.58	0.000284209	0.000165147
4465.82	2614.86	0.000403359	0.000135156
4437.25	2648.78	0.000695039	0.000217871
4408.67	2683.37	0.000598295	0.000195142
4380.1	2718.65	0.000779124	0.000231806
4351.53	2754.62	0.000747044	0.000193871
4322.96	2791.32	0.000629957	0.000218923
4294.39	2828.75	0.000664369	0.000219804
4265.82	2866.94	0.00078652	0.000188504
4237.25	2905.92	0.000612498	0.000219151

4208.67	2945.69	0.000815201	0.000257977
4180.1	2986.29	0.000837538	0.000251901
4151.53	3027.74	0.00114481	0.000251503
4122.96	3070.05	0.000764267	0.000258203
4094.39	3113.26	0.00115293	0.000331217
4065.82	3157.39	0.000956077	0.000277367
4037.25	3202.47	0.00107634	0.000332504
4008.67	3248.52	0.00125737	0.000300387
3980.1	3295.57	0.00145739	0.000311276
3951.53	3343.66	0.00109709	0.000289843
3922.96	3392.81	0.00141262	0.000323132
3894.39	3443.05	0.000938246	0.000359912
3865.82	3494.41	0.00212665	0.000444228
3837.25	3546.94	0.00158055	0.000433683
3808.67	3600.66	0.00114784	0.000423372
3780.1	3655.62	0.00162681	0.000401454
3751.53	3711.85	0.00184145	0.000400394
3722.96	3769.38	0.00173217	0.000442985
3694.39	3828.27	0.00275855	0.00047955
3665.82	3888.55	0.00296811	0.000488053
3637.25	3950.27	0.00206048	0.000434101
3608.67	4013.47	0.00318308	0.000549615
3580.1	4078.2	0.00261873	0.000461125
3551.53	4144.52	0.00233614	0.000472247
3522.96	4212.47	0.00318876	0.000501599
3494.39	4282.11	0.00365572	0.000500051
3465.82	4353.5	0.0043111	0.000499561
3437.25	4426.69	0.00367583	0.00050949
3408.67	4501.75	0.00361488	0.000509221
3380.1	4578.73	0.00501955	0.000545276
3351.53	4657.71	0.00557715	0.000564096
3322.96	4738.76	0.00406336	0.000544933
3294.39	4821.95	0.00616784	0.00058133
3265.82	4907.36	0.00630459	0.000610777
3237.25	4995.06	0.00612178	0.000631382
3208.67	5085.14	0.00586571	0.000660232
3180.1	5177.68	0.0057141	0.000670915
3151.53	5272.78	0.00556075	0.000662922
3122.96	5370.54	0.00460798	0.000633655
3094.39	5471.04	0.00568788	0.000658476
3065.82	5574.41	0.00718243	0.000685879
3037.25	5680.73	0.00715634	0.000676697
3008.67	5790.14	0.00892043	0.000700252
2980.1	5902.75	0.00744903	0.000658966

2951.53	6018.69	0.00661891	0.000658753
2922.96	6138.09	0.0102318	0.000767391
2894.39	6261.09	0.00968651	0.000738672
2865.82	6387.84	0.0113725	0.000813235
2837.25	6518.49	0.0130078	0.00087618
2808.67	6653.2	0.0126728	0.000857348
2780.1	6792.15	0.0127252	0.000890554
2751.53	6935.51	0.0148183	0.00096479
2722.96	7083.48	0.0167889	0.00103746
2694.39	7236.25	0.0160138	0.00103892
2665.82	7394.04	0.0143208	0.00098986
2637.25	7557.07	0.0136226	0.00100424
2608.67	7725.57	0.0131622	0.00101604
2580.1	7899.8	0.01319	0.00102635
2551.53	8080.01	0.012585	0.00101053
2522.96	8266.49	0.0110579	0.00100547
2494.39	8459.52	0.0112736	0.00104376
2465.82	8659.43	0.0125543	0.00108641
2437.25	8866.55	0.00943058	0.00106724
2408.67	9081.22	0.00922956	0.00106297
2380.1	9303.83	0.0090925	0.00114417
2351.53	9534.76	0.00998027	0.00121759
2322.96	9774.44	0.0078995	0.00116936
2294.39	10023.3	0.00861937	0.00127031
2265.82	10281.9	0.00958968	0.00134406
2237.25	10550.7	0.00985538	0.00149635
2208.67	10830.2	0.00777846	0.0015173
2180.1	11121	0.0097274	0.00153843
2151.53	11423.8	0.00611241	0.00141048
2122.96	11739.1	0.00667852	0.00194355
2094.39	12067.9	0.0052622	0.00120184
2037.25	12768.4	0.00509058	0.00124833
1980.1	13532.2	0.0032581	0.00131159
1922.96	14367.2	0.00555226	0.00145937
1865.82	15282.6	0.00414207	0.00176125
1808.67	16289.2	0.00427109	0.00176658
1751.53	17399.6	0.00229554	0.00153351